Received: 12 November 2021 | Revised: 16 March 2022 | Accepted: 17 March 2022

DOI: 10.1002/nbm.4733

RESEARCH ARTICLE

NMR IN BIOMEDICINE WILEY

Quantitative ^{23}Na-MRI of the intervertebral disk at 3 T

Mustafa Çavuşoğlu[1] | Shila Pazahr[2] | Alexander P. Ciritsis[1] | Cristina Rossi[1]

[1]Institute of Diagnostic and Interventional Radiology, University Hospital Zurich, University of Zurich, Switzerland

[2]Balgrist University Hospital, Zurich, Switzerland

Correspondence
Dr Mustafa Çavuşoğlu, Institute of Diagnostic and Interventional Radiology, University Hospital Zürich, Rämistrasse 100, 8091 Zürich, Switzerland.
Email: mustafa.cavusoglu@usz.ch

Funding information
University Hospital Zürich, Grant/Award Number: HYRENEResearchProgram

[Correction added on 19 May 2022, after first online publication: CSAL funding statement has been added.]

Monitoring the tissue sodium content (TSC) in the intervertebral disk geometry noninvasively by MRI is a sensitive measure to estimate changes in the proteoglycan content of the intervertebral disk, which is a biomarker of degenerative disk disease (DDD) and of lumbar back pain (LBP). However, application of quantitative sodium concentration measurements in ^{23}Na-MRI is highly challenging due to the lower in vivo concentrations and smaller gyromagnetic ratio, ultimately yielding much smaller signal relative to ^{1}H-MRI. Moreover, imaging the intervertebral disk geometry imposes higher demands, mainly because the necessary RF volume coils produce highly inhomogeneous transmit field patterns. For an accurate absolute quantification of TSC in the intervertebral disks, the B_1 field variations have to be mitigated. In this study, we report for the first time quantitative sodium concentration in the intervertebral disks at clinical field strengths (3 T) by deploying ^{23}Na-MRI in healthy human subjects. The sodium B_1 maps were calculated by using the double-angle method and a double-tuned (^{1}H/^{23}Na) transceive chest coil, and the individual effects of the variation in the B_1 field patterns in tissue sodium quantification were calculated. Phantom measurements were conducted to evaluate the quality of the Na-weighted images and B_1 mapping. Depending on the disk position, the sodium concentration was calculated as 161.6 mmol/L–347 mmol/L, and the mean sodium concentration of the intervertebral disks varies between 254.6 ± 54 mmol/L and 290.1 ± 39 mmol/L. A smoothing effect of the B_1 correction on the sodium concentration maps was observed, such that the standard deviation of the mean sodium concentration was significantly reduced with B_1 mitigation. The results of this work provide an improved integration of quantitative ^{23}Na-MRI into clinical studies in intervertebral disks such as degenerative disk disease and establish alternative scoring schemes to existing morphological scoring such as the Pfirrmann score.

KEYWORDS
intervertebral disk, quantification, Sodium MRI, x-nuclei

Abbreviations: GRE, gradient echo; PG, proteoglycan; ROI, region of interest; TSC, tissue sodium content.

1 | INTRODUCTION

Back pain is a common medical symptom with massive socioeconomic implications due to effects on the patients' well-being, the inability to work, and the consequential high healthcare costs.[1] Conventional ^{1}H-MRI with morphological sequences is a routinely used imaging technique and provides a tool to rule out common causes such as disk extrusion, degenerative alterations of the facet joints or nerve root compression.[2] However, the symptoms are often unrelated to degenerative findings.[3,4]

Noninvasive quantification of the local sodium content by MRI is a sensitive measure of tissue integrity and a valuable method to monitor the tissue viability and ion homeostasis in clinical research.[5] Both the technological advancements on the hardware side of MRI and the emergence of efficient data acquisition techniques (such as ultra-short echo-time—T_E—sequences) have enabled the utilization of ^{23}Na-MRI as a potential tool to directly infer functional and structural information on the tissue, otherwise not achievable by conventional ^{1}H-MRI.[6–8]

Previous studies have shown that the sodium content in the disks correlates with the proteoglycan (PG) content, which in turn seems to be a biomarker of degenerative disk disease (DDD) and of lumbar back pain (LBP).[9,10] Histologically, the intervertebral disk consists of an outer annulus fibrosus and an inner nucleus pulposus. Biochemically, these components are largely composed of collagen and PG. The negative fixed charge density attracts sodium ions, resulting in the concentration of sodium within the disk being directly proportional to the fixed charge density.[11] The pathologic and degenerative reduction of PG content and attraction of positively charged sodium ions causes a lower oncotic pressure and ultimately collagen degeneration. Therefore, ^{23}Na-MRI is a sensitive method to estimate the changes in the PG content of the intervertebral disk, similar to the articular cartilage.[12,13]

Although ^{23}Na-MRI offers valuable supplementary information to ^{1}H-MRI, the practical implementation of tissue sodium quantification poses high demands on the measurement accuracy and precision. First, the signal-to-noise ratio of ^{23}Na-MRI is significantly lower than that of ^{1}H-MRI. This is mainly because the sodium concentration in the tissue is much lower (45 mM to 350 mM) relative to the water concentration and the gyromagnetic ratio is smaller ($\gamma_H/\gamma_{Na} \approx 3.7$), ultimately yielding an 11 000 times smaller ^{23}Na signal relative to ^{1}H-MRI, under equivalent detection conditions for the two nuclei.[14] Second, as a spin-3/2 nucleus, ^{23}Na signal poses rapid biexponential transverse relaxation[15] and may also exhibit energy eigenstate shifting (or residual quadrupole splitting) as a result of the local electric field gradients due to the long-lived spatial orientation of the nuclear electric quadrupole moment.[16,17] Third, blurring results from the point spread function and from physiological motion. Fourth, strong partial volume effects because of the large voxel sizes lead to further inaccuracies. Finally, the signal modulation due the inhomogeneity in the B_1 field appears as a significant challenge for the accurate quantification.[18,19] The quantification of the tissue sodium content (TSC) in units of millimoles per liter potentially allows the inter- and intra-individual comparability necessary for patient stratification and for therapy monitoring.[20] However, quantitative analysis of sodium concentration from ^{23}Na-MRI requires accurate control of factors modulating the sodium signal.[21]

Primarily, the accuracy and precision of the quantitative tissue sodium measurement are highly dependent on the spatial and temporal modulation of all the magnetic fields involved in the experimental realization. Significant error can be introduced due to B_1 inhomogeneity in TSC measurement.[18,19] A common approach to overcome this issue in ^{1}H-MRI is to use a relatively homogeneous transmit coil (such as a quadrature birdcage) by assuming that variations in flip angle are small in the imaging volume.[22] However, if body-volume coils or other highly inhomogeneous transmit coils must be used, this is not applicable and B_1 inhomogeneity has to be included in the quantification model. The specific geometry of the intervertebral disks and necessary antenna specs to image this geometry push the accuracy demand in quantification. Therefore, particularly for the intervertebral disks, B_1 field variations have to be mitigated by adequate correction methods to perform a reliable tissue sodium quantification.

The goal of this work is to provide quantitative TSC measurements using ^{23}Na-MRI in a clinical setting by taking into account the effects of spatial variations in the B_1 field along and across the intervertebral disk anatomy. To this end, ^{23}Na-MRI was performed to image the intervertebral disks at 3 T in healthy human subjects. The sodium B_1 maps were acquired with a double-tuned (^{1}H/^{23}Na) transceive chest coil and their individual effects in tissue sodium quantification were examined.

2 | EXPERIMENTAL

2.1 | MRI hardware

All measurements were made on a 3 T whole-body MRI scanner (MAGNETOM Skyra, Siemens Healthcare, Erlangen, Germany). A dual-tunable (^{1}H/^{23}Na) chest coil (Rapid Biomedical, Rimpar, Germany) was used for transmission and reception of ^{23}Na and ^{1}H signal. The built-in body coil was used for ^{1}H signal excitation. The operation frequency of the antenna is 32.6 MHz for ^{23}Na nuclei and 123.2 MHz for protons. The coil is composed mainly from three modular components: an upper component (2 Tx ^{23}Na, 2 Tx ^{1}H), a flexible component (2 Rx ^{23}Na, 2 Rx ^{1}H) and a bottom component (2 Tx ^{23}Na, 2ch Rx ^{23}Na). The volume coil (top and bottom components) size is 57 (length) × 49 (width) × 37 (height) cm^3 and the flexible receive coil size is 30 (length) × 35 (width) × 35 (height) cm^3. The software for the pulse sequence allows us to operate the coil at either sodium or proton frequency.

2.2 | Study participants

Written informed consent was obtained from six participants. The ethical board of the institution approved the study and all volunteers provided information prior to the examination. Due to macroscopic motion, data from one subject were rejected. Imaging with the same protocol was performed in the intervertebral disks of a total of five healthy volunteers (two males and three females) with an average age of 29.1 ± 4.2 years.

2.3 | Phantom measurements

To evaluate the distribution of B_1 field in a homogeneous medium, cylindrical phantom measurements were acquired. The phantom measurements were made using a volume cylindrical polyethylene container filled with 150 mmol/L NaCl. The same protocol and data processing as detailed below were applied. Additionally, five cylindrical phantom tubes filled with 50, 100, 150, 200 and 250 mmol/L NaCl with 5% agarose gel were used as a reference sodium signal intensity in experiments. The phantoms were located at the center of the volume coil and sodium concentration measurements were made with and without B_1 field correction to validate the applied ^{23}Na imaging protocol and quantification framework.

2.4 | MRI protocol

2.4.1 | RF pulse calibration

A global RF pulse calibration was performed by adjusting the transmitter voltages between 200 and 340 V (15 measurements with linearly increasing nominal flip angle from 0° to 180°) using a nonlocalized rectangular 1 ms length RF pulse to ensure a true 90° flip angle at the center of the coil geometry before all measurements.

2.4.2 | ^{23}Na-MRI

Following a survey, sagittal and coronal ^{1}H images were acquired for accurate positioning of the intervertebral disk. The spin-density-weighted ^{23}Na images were acquired using a gradient echo (GRE) pulse sequence with the following parameters in supine position: $T_R/T_E = 320/1.98$ ms, FOV = 320 × 320 mm^2, voxel size = 5 × 5 × 10 mm^3, number of slices = 3, NEX = 128, nominal flip angle = 90°, total acquisition time = 5.56 min.

2.4.3 | ^{1}H-MRI

T_1- and T_2 -weighted ^{1}H anatomical imaging protocol was performed to facilitate image segmentation. The same coil was used for excitation and signal reception for ^{1}H-MRI without repositioning the subject. A FLASH sequence was used to acquire the T_1-weighted structural scan ($T_R/T_E = 308/4.77$ ms, 24 interleaves, FOV = 320 × 320 mm^2, voxel size = 1 × 1 × 1 mm^3).

2.4.4 | B_1 field mapping

The contrast variation of the ^{23}Na-MRI is fundamentally determined by the RF coils used for signal excitation and reception, and as expected the B_1 field patterns can drastically change based on the antenna involved. Sodium B_1 mapping was performed using the double-angle method, which encodes the flip angle into the amplitude of the complex MRI signal.[23] The B_1 field distribution is determined by the ratio of two images obtained at different nominal flip angles α_0 and $2\alpha_0$. The field map $\alpha(r)$ was calculated based on the relationship between the effective and nominal flip angles from two GRE volumes acquired with 45° and 90° flip angles:

$$\alpha(r) = \arccos\left(\left|\frac{I_{90}(r)}{2I_{45}(r)}\right|\right) \quad (1)$$

where I_{45} and I_{90} are the intensities of the corresponding voxels in images acquired with 45° and 90° flip angles. A long repetition time ($T_R = 100$ ms) was used to minimize the T_1 dependence in B_1 mapping. Note that only the transceive coil was considered, and based on the

principle of reciprocity both transmit and reception field amplitudes are denoted as B_1 in this study. The flip angle maps were calculated on a voxel-by-voxel basis across the imaging volume. The correction factor was calculated for every voxel by dividing the actual flip angle obtained from the flip angle map by the nominal flip angle, and the resulting correction factor was applied to mitigate the B_1 inhomogeneity on the sodium images.

2.5 | Sodium quantification

Sodium concentration quantification is usually done by placing reference phantoms with known sodium concentrations and relaxation times within the field of view of the images (i.e., the ranges of the reference tubes are usually 10 mM–150 mM to image brain or muscle, 100 mM–350 mM for cartilage).[20] In the volunteer measurements, five standardized reference sodium tubes were included in the field of view to allow quantification of the TSC. Moreover, internal tissue references such as cerebrospinal fluid with a well defined sodium concentration of 150 mM/L were used as a reference and for validation.[24]

2.6 | Image processing and data analysis

Subsequent data processing and analysis were carried out using self-developed scripts in MATLAB (MathWorks, Natick, MA, USA). TSC was calculated via an intensity calibration curve fitted to the signal of the reference tubes and the linear regression curve was used to extrapolate the sodium maps of the intervertebral disks. To minimize the influence of B_1 inhomogeneity on ^{23}Na-MRI, particularly in the specified geometry, all sodium-weighted images were subjected to voxel-wise B_1-field correction. In vivo TSC values are presented as mean and standard deviation in millimoles per liter. To determine a region of interest (ROI) of intervertebral disks, T_1-weighted ^{1}H images were used. Intensity thresholding was performed after plotting the border contours, resulting in a binary mask, where individual intervertebral disks were identified. The identified binary masks defining the intervertebral disks were controlled by an external radiologist. The B_1 inhomogeneity corrected TSC maps were calculated with in the identified intervertebral disks.

In vivo quantitative TSC values for each subject are presented as mean and standard deviation in millimoles per liter. A paired-sample t-test was performed to compare the mean sodium concentrations of different subjects for the uncorrected and B_1 corrected cases.

3 | RESULTS

The dual-tunable (^{1}H/^{23}Na) chest coil used for reception of ^{1}H, and for transmission and reception of ^{23}Na signals, is shown in Figure 1A. Figure 1B shows a simulation of transmit field efficiency of the coil in the transverse axis illustrating that, while the B_1 field has relatively homogeneous pattern in the close vicinity of the transmit elements, it decreases towards the center of the coil. Figure 1C shows a spin-density-weighted sagittal image of the intervertebral disk geometry used as a localizer. The intensity variations on the image as a result of field inhomogeneity are observable. The five reference tubes were placed in the field of view with varying sodium concentrations. Figure 1D shows the flip angle map for proton signal, exhibiting a relatively high SNR in the intervertebral disks but poor SNR between the disks along the spine. The nonuniformity of the transmit field for protons is also visible on the reference tubes.

Figure 2 shows the effect of B_1 field in quantitative sodium imaging in a homogeneous phantom. Figure 2A shows the sodium concentrations of the reference tubes and the imaging phantom. Five reference tubes with 50 mmol/L, 100 mmol/L, 150 mmol/L, 200 mmol/L and 250 mmol/L NaCl with 5% agarose were placed above the imaging phantom with the sodium concentration of 150 mmol/L. Figure 2B shows the Na image of the phantoms with arbitrary units where the concentration gradient of the reference tubes from left to right is nicely depicted. Figure 2C shows the sodium flip angle map acquired with a double angle method (actual flip angle divided by the nominal flip angle). Even though the phantom and the reference tubes were placed at the center of the coil geometry and the imaging volume is much smaller compared with a human subject, there is up to 15% field nonuniformity across the phantom. The corresponding TSC maps with and without B_1 field correction are illustrated in Figure 2D and 2E respectively. The color bar refers to the actual sodium concentrations within the tubes and the phantom, demonstrating that the true concentrations were accurately reconstructed from the ^{23}Na-MR images. The effect of B_1 field correction is depicted in Figure 2F as the bar graphs of the B_1 field corrected and uncorrected concentrations within the tubes and the phantom. While the B_1 field exhibits relatively small variation within the imaging phantom, around 5%, the inhomogeneity increases along the reference tubes up to 15%, as implied by the flip angle map.

Figure 3 shows the ROI placement using the T_1-weighted ^{1}H images. Figure 3A shows the T_1-weighted image, where the individual intervertebral disk structures are clearly visible. Figure 3B shows the intensity thresholding of the T_1-weighted structural image within the determined contours along the spine and the binary mask extracted from the thresholded images that is used as the ultimate ROI to calculate the TSC within

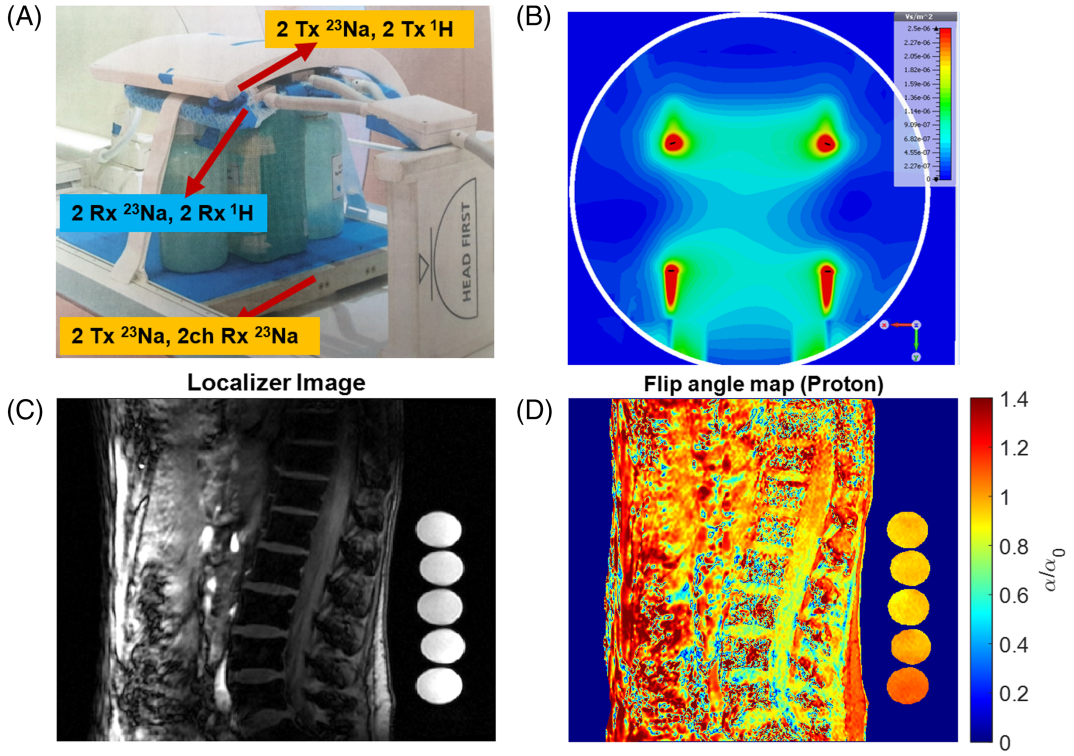

FIGURE 1 RF coil and proton field sensitivity. A, The dual-tunable (^{1}H/^{23}Na) chest coil: the operation frequency of the ^{1}H is 123.2 MHz and that for ^{23}Na is 32.6 MHz. The coil is composed mainly from three modular components: an upper component (2 Tx ^{23}Na, 2 Tx ^{1}H), a flexible component (2 Rx ^{23}Na, 2 Rx ^{1}H) and a bottom component (2 Tx ^{23}Na, 2ch Rx ^{23}Na). The volume coil (top and bottom components) size is 57 (length) × 49 (width) × 37 (height) cm^3 and the flexible receive coil size is 30 (length) × 35 (width) × 35 (height) cm^3. B, Simulation of transmit field efficiency of the coil (V/m^2) in the transverse axis, showing that, while the B_1 field has relatively homogeneous pattern in the close vicinity of the transmit elements, it decreases towards the center of the coil. C, Localizer image of the intervertebral disks obtained as a spin-density weighted sagittal image. D, Flip angle map for proton signal using the body coil for transmission and the receiver elements of the rapid coil for reception exhibiting a relatively homogeneous transmit and receive field sensitivity with a relatively high SNR in the intervertebral disks but poor SNR between the disks

the intervertebral disks. The intervertebral disks from T9/T10 to L5/S1 are labelled on the image. Figure 3C shows the ROI for CSF identified on the structural image as the internal tissue reference and validation of the sodium concentration measurement. Figure 3D illustrates the quantitative TSC map, illustrating that the sodium concentrations in the CSF were measured as 148 ± 7 within the defined ROI and the sodium concentrations within the intervertebral disks were accurately quantified based on the references.

Figure 4 presents the effect of B_1 field in quantitative sodium imaging in an exemplary subject. Figure 4A shows ^{23}Na images, where the sodium content of the intervertebral disks is clearly depicted in arbitrary units. The limited SNR provided by the utilized antenna prevents us imaging the whole spine structure at the same time. Figure 4B shows the in vivo sodium flip angle map depicted as the ratio of the actual to the nominal flip angle, which was deployed as the voxel-by-voxel correction factor. The magnetic field nonuniformity was measured up to 40% depicted by the flip angle map along and across the intervertebral disk geometry. Figure 4C and 4D shows the in vivo quantitative sodium concentration maps without and with B_1 field correction respectively. Even though a limited resolution was provided by the ^{23}Na-MRI, the anatomical structure of the intervertebral disks can be identified as annulus fibrosus and nucleus pulposus from the quantitative TSC maps. A further observation yielded by Figure 4D is that, even though the B_1 field variations were corrected, the quantitative TSC values are varying among the individual disks along the spine, which potentially signals physiological roots.

The mean sodium concentration values are listed in Table 1 and Table 2 for B_1 uncorrected and corrected cases respectively for the individual disks. Depending on the disk position, the sodium concentration was calculated as 161.6 mmol/L–347 mmol/L and the mean sodium concentration of the intervertebral disks varies between 254.6 ± 54 mmol/L and 290.1 ± 39 mmol/L after B_1 correction. We observed a significant ($p < 0.005$) difference in the TSC after B_1 correction. Among individual disks of the same subject, the TSC values are significantly ($p < 0.001$) different compared with each other. In all subjects, there is a significant decrease in standard deviation of the mean sodium concentration with B_1 corection.

Figure 5 shows quantitative analysis of TSC within the individual disks and among different subjects. Figure 5A shows the variation of the average TSC values among the individual disks for a representative subject and the effect of B_1 field correction on it. While the effect of

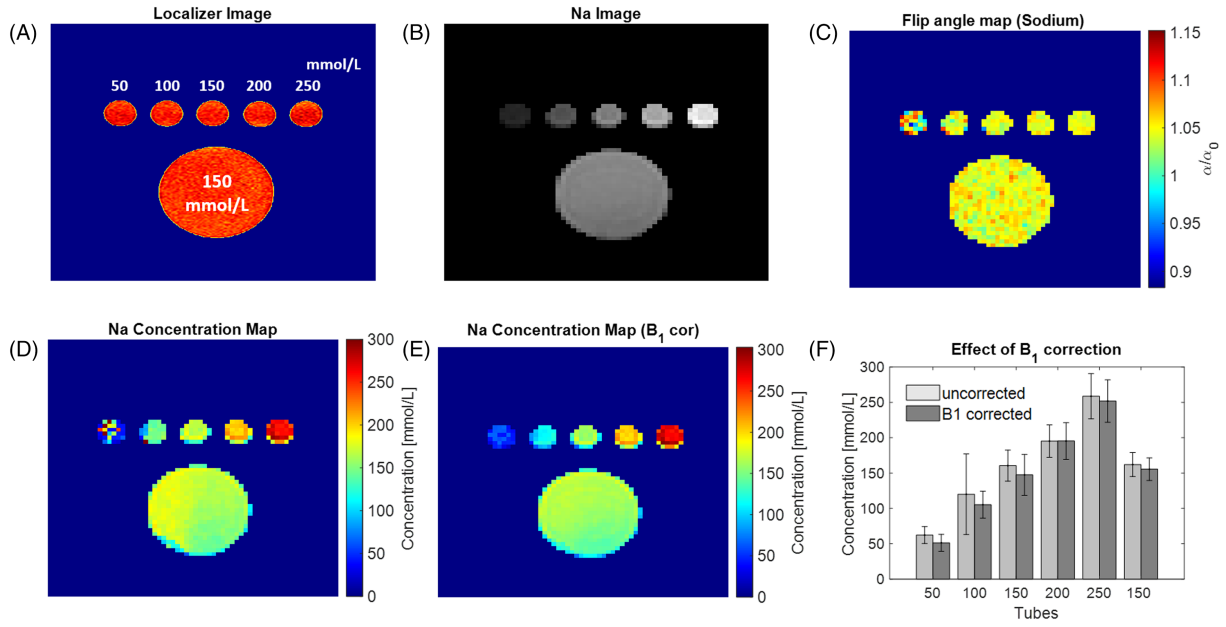

FIGURE 2 Effect of B_1 field in quantitative sodium imaging in a homogeneous phantom. A, Placement of the reference tubes with 50 mmol/L, 100 mmol/L, 150 mmol/L, 200 mmol/L and 250 mmol/L NaCl with 5% agarose and the imaging phantom with the sodium concentration of 150 mmol/L. B, Na image of the phantoms with arbitrary units where the concentration gradient of the reference tubes from left to right is depicted. C, Sodium flip angle map illustrated as the ratio of actual flip angle divided by the nominal flip angle. There is a B_1 field nonuniformity across the phantom up to 15% even though the phantom and the reference tubes were placed at the center of the coil geometry and the imaging volume is much smaller compared with a human subject. D, Quantitative TSC maps without B_1 field correction. E, Quantitative TSC maps with B_1 field correction. The color bar refers to the actual sodium concentrations within the tubes and the phantom, demonstrating that the true concentrations were accurately reconstructed from the ^{23}Na-MR images. F, bar graphs of the B_1 field corrected and uncorrected concentrations within the tubes and the phantom. While the B_1 field exhibits relatively small variation within the imaging phantom, around 5%, the inhomogeneity increases along the reference tubes up to 15% as implied by the flip angle map

correction is relatively small for the disks positioned in the middle of the imaging volume (L1/L2, L2/L3, L3/L4), there is a prominent effect for the remaining disks located relatively close to the periphery of the imaging volume. Figure 5B shows the B_1 corrected TSC variation among the individual disks for different subjects. It is highly noticeable that the variation of TSC along the disks for different subjects provides similar patterns, yielding an increasing tendency from T9/T10 until L2/L3, where it peaks, and a decreasing pattern for the lower lumbar disks. Figure 5C shows the effect of B_1 field correction on the mean TSC of individual subjects (average of mean TSC for all disks for a single subject). The smoothing effect of B_1 correction by reducing the standard deviation in the average TSC for each subject is clear. Figure 5D shows the variation of normalized TSC (the ratio of TSC at each disk normalized by the mean TSC of all the disks for a single subject) for different subjects. As an analogy to coefficient of variation, the normalized TSC variation provides highly horizontal curves, implying a convergence to a constant ratio for every subject, varying between 0.6 and 1.3 for different disks.

4 | DISCUSSION

In principle, in order to ensure an accurate quantitative TSC measurement, the acquired ^{23}Na signal must be corrected for all contrast mechanisms apart from sodium concentration. The functional information extracted from the Na images can only be reliably applied if all signal modulations are well defined. The B_1 field at the sodium Larmor frequency emitted from a typical body-volume antenna poses significant magnetic field inhomogeneity along the spine, directly affecting the spin evolution and ultimately the ^{23}Na signal. In this study, we reported for the first time quantitative sodium concentrations in the intervertebral disks at clinical field strengths (3 T) by deploying ^{23}Na-MRI in healthy human subjects. This study is also the first to present sodium B_1 mapping in intervertebral disks and to assess the effect of sodium B_1 mapping to the quantitative TSC.

Dual resonant coils such as the one used in this work for sodium imaging are attractive mainly because they allow reference ^{1}H images to be acquired without repositioning the subject. In contrast to quadrature birdcage coils, which usually provide relatively homogeneous excitation field patterns at 3 T, the body-volume coils covering the intervertebral disk geometry exhibit highly inhomogeneous B_1 field profiles. Additionally, anatomical variations that differ in electrical permittivity from surrounding tissue further exacerbate the B_1 nonuniformities. The double-angle method was used to calculate the flip angle maps due to easy practical implementation for sodium B_1 mapping. There are several other B_1

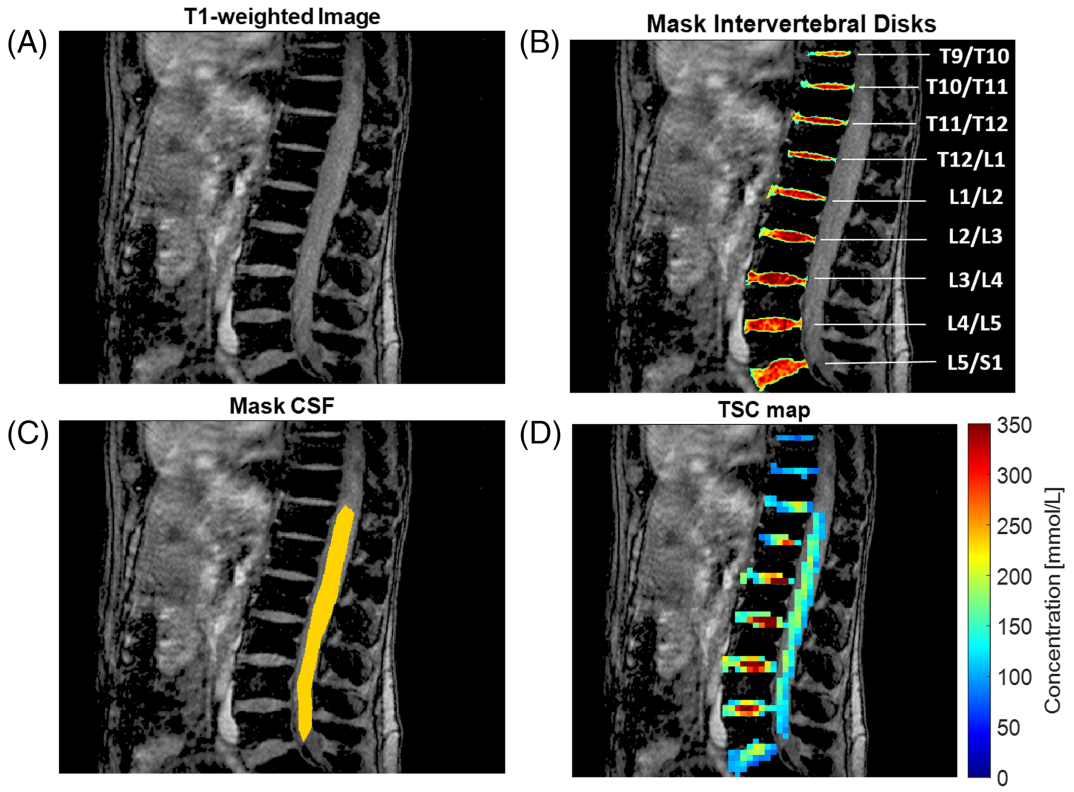

FIGURE 3 ROI placement and TSC quantification. A, T_1-weighted image of the intervertebral disks where the individual disk structures is clearly visible. B, Intensity thresholding of the T_1-weighted structural image within the determined contours along the spine. The mask extracted from the thresholded images is used as the ultimate ROI. The intervertebral disks from T9/T10–L5/S1 are labelled. C, The ROI for CSF identified on the structural image. The Na concentration of the CSF was used as the internal tissue reference and validation of the sodium concentration measurements. D, The quantitative TSC map, illustrating that the sodium concentrations in the CSF were measured as 148 ± 7 within the defined ROI and the sodium concentrations within the intervertebral disks were accurately quantified based on the references

mapping techniques that could potentially be utilized such as actual flip-angle imaging,[25] Bloch–Siegert shift[26] or the phase-sensitive method.[19] In comparison studies, it was previously reported that the Bloch–Siegert shift method and phase-sensitive method are the most accurate methods for ^{1}H.[27,28] For ^{23}Na-MRI, the phase-sensitive method is shown to yield higher quality B_1 maps at low signal-to-noise ratio and greater consistency of measurement than the double-angle method, but with higher vulnerability to large off-resonance shifts. Recently, a method for simultaneous B_1 mapping and imaging was proposed in order to enhance accuracy and to reduce measurement time with higher SNR compared with the double-angle method, which could potentially be applied.[18]

To mitigate problems associated with low signal levels obtained during in vivo sodium imaging and sodium B_1 mapping experiments, the image resolution was limited to pixel sizes of a few millimeters ($5 \times 5 \times 10\,mm^3$). However, such a voxel volume causes the accuracy of ^{23}Na-MRI to be strongly biased by partial volume effects (PVEs). Previously reported partial volume correction (PVC) methods for ^{23}Na-MRI for the brain tissue could be adapted for the spinal cord geometry.[29]

Phantom measurements were conducted to evaluate the quality of the Na-weighted images and B_1 mapping. The experiments showed that the B_1 correction could significantly improve the quantitative accuracy of the sodium concentration maps besides smoothing the excitation profile, implied by the reduced standard deviation. Thus we performed B_1 correction for the in vivo data. In previous work concerning the ^{23}Na-MRI in the head using a transceive birdcage coil, B_1 correction had up to 10% difference in TSC for white matter, cerebrospinal fluid and vitreous humour.[18] The larger influence of the B_1 correction on the measured TSC values that was observed in our work is caused by the higher B_1 non-uniformity profile of the body-volume coil used. The sodium concentration values of the intervertebral disk of 161.6 mmol/L–347.0 mmol/L agree with previous studies using sodium MRS.[30–32] After the application of B_1 mitigation, the standard deviation of the mean sodium concentration was significantly reduced ($p < 0.001$) and the smoothing effect of the B_1 correction is obvious.

^{23}Na-MRI is a promising quantitative method that might be helpful to determine the biochemical status of the human intervertebral disk and better understand the pathophysiology of disk degeneration.[21] Previous studies have reported that a T_2-weighted semiquantitative grading system and Pfirrmann classification can be used for the assessment of healthy and degenerative disks.[33,34] In the clinical routine, measurement of sodium representing the PG content of the disk might provide a noninvasive tool for assessment of disk degeneration at an early stage, giving the

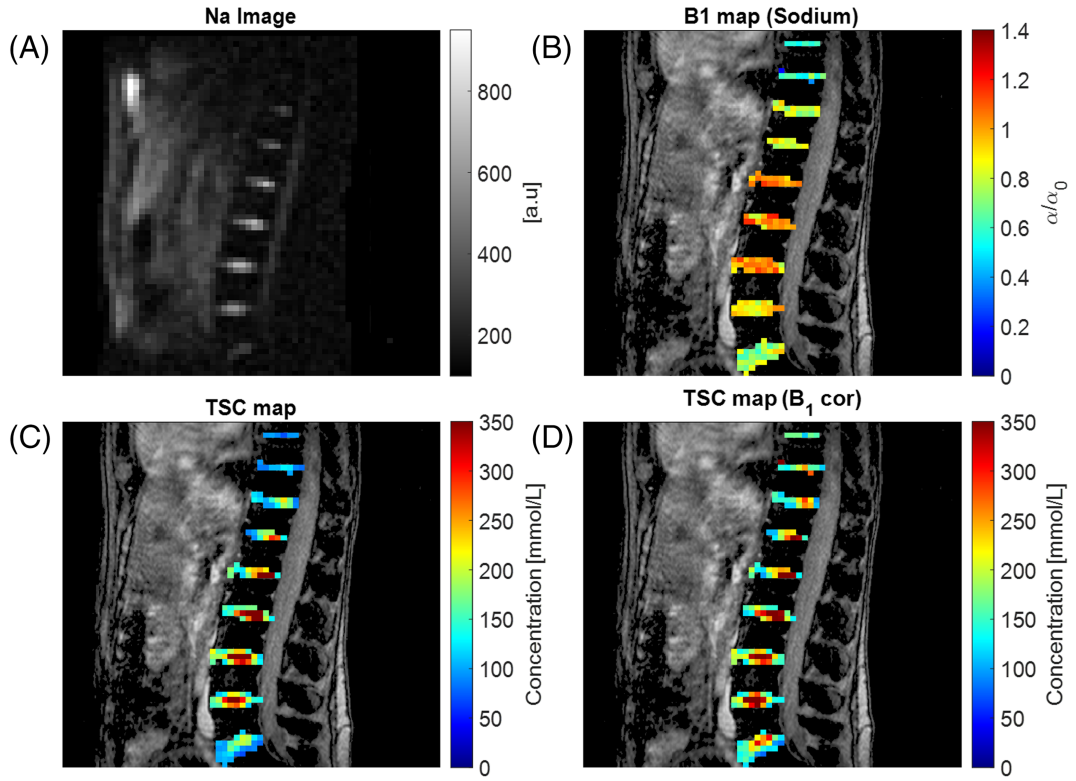

FIGURE 4 Effect of B_1 field in quantitative sodium imaging in an exemplary subject. A, ^{23}Na images, where the sodium content of the intervertebral disks is clearly depicted in arbitrary units. The limited SNR provided by the utilized antenna prevents us imaging the whole spine structure at the same time. B, The in vivo sodium flip angle map depicted as the ratio of the actual to the nominal flip angle, which was further deployed as the voxel-by-voxel correction factor. The magnetic field nonuniformity was measured up to 40% depicted by the flip angle map along the intervertebral disk geometry. C, In vivo quantitative sodium concentration maps without B_1 field correction. D, In vivo quantitative sodium concentration maps with B_1 field correction. Even though a limited resolution was provided by the ^{23}Na-MRI, the anatomical structure of the intervertebral disks can be identified as annulus fibrosus (outer shell) and nucleus pulposus (inner shell) from the quantitative TSC maps. Even though the B_1 field variations were corrected, the quantitative TSC values are varying among the individual disks along the spine, potentially caused by physiological factors

TABLE 1 Average quantitative sodium concentrations in the individual disks [mmol/L] calculated in the ROIs for each subject without B_1 field correction

IV disks	S1	S2	S3	S4	S5
T9/T10	136.5 ± 12	140.5 ± 15	134.6 ± 14	145.8 ± 16	148.4 ± 14
T10/T11	147.7 ± 18	207.2 ± 31	168.3 ± 19	197.2 ± 16	166.2 ± 20
T11/T12	193.8 ± 15	184.1 ± 24	211.2 ± 27	218.5 ± 27	207.4 ± 33
T12/L1	255.0 ± 33	276.5 ± 49	243.1 ± 28	257.5 ± 32	301.2 ± 41
L1/L2	298.0 ± 53	301.7 ± 39	324.0 ± 41	291.4 ± 49	316.2 ± 49
L2/L3	349.8 ± 63	321.3 ± 44	345.0 ± 51	306.5 ± 43	332.4 ± 52
L3/L4	344.4 ± 51	341.6 ± 52	319.8 ± 49	233.0 ± 34	253.2 ± 32
L4/L5	302.5 ± 42	268.8 ± 32	175.2 ± 21	198.5 ± 16	193.8 ± 26
L5/S1	174.9 ± 20	219.1 ± 28	150.2 ± 19	116.5 ± 10	145.2 ± 17
Mean ± std	244.7 ± 83	251.2 ± 67	230.1 ± 81	213.3 ± 62	229.3 ± 73

possibility for prevention and to monitor treatment effects, providing a quantitative tool. The quantitative sodium concentration in the intervertebral disks at clinical field strengths provided in this work with correction of the transmit field variations further improves the accuracy of the overall clinical ^{23}Na-MRI framework.

TABLE 2 Average quantitative sodium concentrations in the individual disks [mmol/L] calculated in the ROIs for each subject with B_1 field correction

IV disks	S1	S2	S3	S4	S5
T9/T10	199.5 ± 28	221.2 ± 29	204.7 ± 19	216.2 ± 17	200.7 ± 18
T10/T11	237.0 ± 21	268.8 ± 46	225.9 ± 22	234.1 ± 19	221.5 ± 21
T11/T12	245.1 ± 22	288.4 ± 48	250.2 ± 29	266.5 ± 37	246.1 ± 42
T12/L1	312.0 ± 48	304.5 ± 43	252.6 ± 30	288.5 ± 51	327.6 ± 51
L1/L2	293.8 ± 50	320.5 ± 45	300.0 ± 54	276.5 ± 46	334.8 ± 87
L2/L3	348.0 ± 57	347.0 ± 56	333.6 ± 59	340.6 ± 25	339.8 ± 56
L3/L4	337.9 ± 51	326.2 ± 43	328.2 ± 47	313.8 ± 32	260.4 ± 34
L4/L5	343.5 ± 43	288.4 ± 28	213.4 ± 28	197.5 ± 17	268.2 ± 36
L5/S1	231.3 ± 34	246.4 ± 30	183.2 ± 23	161.6 ± 13	259.2 ± 25
Mean ± std	283.1 ± 55	290.1 ± 39	254.6 ± 54	255.0 ± 57	268.4 ± 45

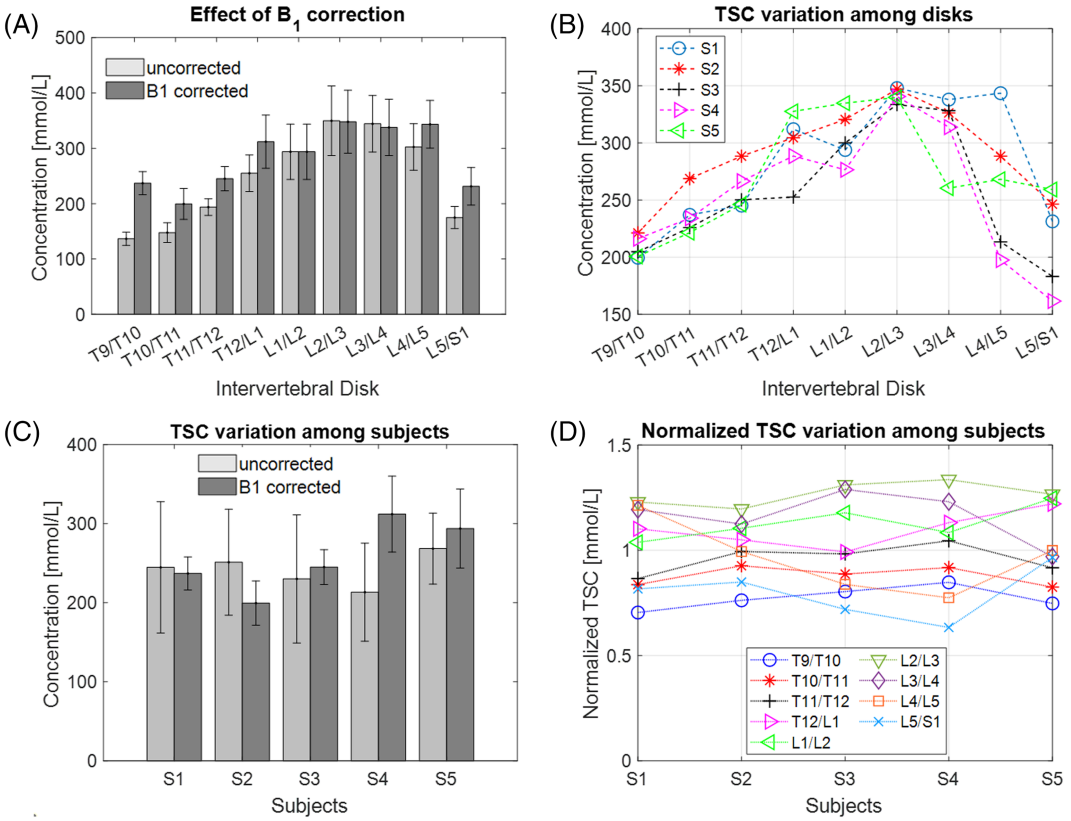

FIGURE 5 Quantitative analysis of TSC within the individual disks and among different subjects. A, The variation of the average TSC values among the individual disks for a representative subject and the effect of B_1 field correction on it. B, B_1 corrected TSC variation among the individual disks for different subjects. It is highly noticeable that the variation of TSC along the disks for different subjects provides similar patterns, yielding an increasing tendency from T9/T10 until L2/L3 where it peaks and a decreasing pattern for the lower lumbar disks. C, Effect of B_1 field correction on the mean TSC of individual subjects (average of mean TSC for all disks for a single subject). D, Variation of normalized TSC (the ratio of TSC at each disk normalized by the mean TSC of all the disks for a single subject) for different subjects. As an analogy to coefficient of variation, the normalized TSC variation provides highly horizontal curves, implying a convergence to a constant ratio for every subject varying between 0.6 and 1.3 for different disks

This study has some limitations concerning the technical aspects. First of all, no B_0 correction was performed. Although the B_0 maps we obtained from the phantom measurements exhibit negligible off-resonance (below 3 Hz), susceptibility artifacts are highly prevalent along the spinal cord due to different susceptibilities in the intervertebral disks, and the lungs cause significant variations in the B_0 field. However, the B_0 shimming is highly challenging in the spinal cord geometry using the standard shim procedure mainly because not all inhomogeneity can be

compensated with only first- and second-order shim coils.[35] Higher order shimming and slice-wise dynamic shimming are needed for sufficient compensation.[36] Moreover, the dynamic variation of the B_0 field due to the respiration cycle and moving dielectric tissue such as chest and abdomen can cause significant field fluctuations that require dynamic higher order shimming.[37] It has been previously reported that in vivo ^{23}Na nucleus exhibits a fast biexponential transversal relaxation time such that 60% of the signal decays with a T_2^* of 0.7–3 ms (fast component) and 40% of the signal decays with a T_2^* of 16–20 ms (slow component).[38] Consequently, it is important to acquire images at a short T_E to avoid the signal loss from the fast-relaxing component. We acquired images at 1.98 ms, leading to a residual T_2^* weighting of the signal that can be further reduced by using ultra-short echo time acquisition schemes.[7,8] Regarding this study, limitations include the small number of participants as well as missing reproducibility assessment. Both tasks will be taken as future work, particularly to study the short- and mid-term variability of the sodium concentration measurement in the intervertebral disks, which is most interest for clinical studies to monitor variations due to underlying physiological dynamics.

5 | CONCLUSION

In conclusion, quantitative ^{23}Na-MRI is a promising tool to measure clinically relevant longitudinal changes in the intervertebral disks. Here, we reported quantitative sodium concentration measurement in the intervertebral disks at clinical field strengths (3 T). We showed that the B_1 nonuniformities associated with the antenna utilized for imaging significantly modulate the ultimate TSC and have to be mitigated for quantitative sodium concentration mapping. The results of this work have the potential to enable an improved integration of quantitative ^{23}Na-MRI into clinical studies in intervertebral disks such as degenerative disk disease and establish alternative scoring schemes to existing morphological scoring such as the Pfirrmann score.

ACKNOWLEDGEMENTS

Open Access Funding provided by Universitat Zurich.

ORCID

Alexander P. Ciritsis https://orcid.org/0000-0003-0920-9700
Cristina Rossi https://orcid.org/0000-0002-9041-2222

REFERENCES

1. Fatoye F, Gebrye T, Fatoye C, et al. The clinical and cost-effectiveness of telerehabilitation for people with nonspecific chronic low back pain: randomized controlled trial. *JMIR mHealth uHealth*. 2020;8(6):e15375. doi:10.2196/15375
2. Fries P, Runge VM, Kirchin MA, Watkins DM, Buecker A, Schneider G. Magnetic resonance imaging of the spine at 3 Tesla. *Semin Musculoskelet Radiol*. 2008;12(3):238-252. doi:10.1055/s-0028-1083107
3. Balague F, Mannion AF, Pellise F, Cedraschi C. Non-specific low back pain. *Lancet*. 2012;379(9814):482-491. doi:10.1016/S0140-6736(11)60610-7
4. Weishaupt D, Zanetti M, Hodler J, Boos N. MR imaging of the lumbar spine: prevalence of intervertebral disk extrusion and sequestration, nerve root compression, end plate abnormalities, and osteoarthritis of the facet joints in asymptomatic volunteers. *Radiology*. 1998;209(3):661-666. doi:10.1148/radiology.209.3.9844656
5. Madelin G, Lee JS, Regatte RR, Jerschow A. Sodium MRI: methods and applications. *Prog Nucl Magn Reson Spectrosc*. 2014;79:14-47. doi:10.1016/j.pnmrs.2014.02.001
6. Boada FE, Gillen JS, Shen GX, Chang SY, Thulborn KR. Fast three dimensional sodium imaging. *Magn Reson Med*. 1997;37(5):706-715. doi:10.1002/mrm.1910370512
7. Nielles-Vallespin S, Weber MA, Bock M, et al. 3D radial projection technique with ultrashort echo times for sodium MRI: clinical applications in human brain and skeletal muscle. *Magn Reson Med*. 2007;57(1):74-81. doi:10.1002/mrm.21104
8. Nagel AM, Laun FB, Weber MA, Matthies C, Semmler W, Schad LR. Sodium MRI using a density-adapted 3D radial acquisition technique. *Magn Reson Med*. 2009;62(6):1565-1573. doi:10.1002/mrm.22157
9. Luoma K, Riihimaki H, Luukkonen R, Raininko R, Viikari-Juntura E, Lamminen A. Low back pain in relation to lumbar disc degeneration. *Spine*. 2000;25(4):487-492. doi:10.1097/00007632-200002150-00016
10. An HS, Anderson PA, Haughton VM, et al. Introduction: disc degeneration: summary. *Spine*. 2004;29(23):2677-2678. doi:10.1097/01.brs.0000147573.88916.c6
11. Shapiro EM, Borthakur A, Gougoutas A, Reddy R. ^{23}Na MRI accurately measures fixed charge density in articular cartilage. *Magn Reson Med*. 2002;47(2):284-291. doi:10.1002/mrm.10054
12. Borthakur A, Mellon E, Niyogi S, Witschey W, Kneeland JB, Reddy R. Sodium and $T_{1\rho}$ MRI for molecular and diagnostic imaging of articular cartilage. *NMR Biomed*. 2006;19(7):781-821. doi:10.1002/nbm.1102
13. Insko EK, Clayton DB, Elliott MA. In vivo sodium MR imaging of the intervertebral disk at 4 T. *Acad Radiol*. 2002;9(7):800-804. doi:10.1016/s1076-6332(03)80350-1
14. Madelin G, Regatte RR. Biomedical applications of sodium MRI in vivo. *J Magn Reson Imaging*. 2013;38(3):511-529. doi:10.1002/jmri.24168
15. Stobbe RW, Beaulieu C. Exploring and enhancing relaxation-based sodium MRI contrast. *Magn Reson Mater Phys Biol Med*. 2014;27(1):21-33. doi:10.1007/s10334-013-0390-7

16. Tsang A, Stobbe RW, Beaulieu C. In vivo double quantum filtered sodium magnetic resonance imaging of human brain. *Magn Reson Med*. 2015;73(2):497-504. doi:10.1002/mrm.25131
17. Kordzadeh A, Duchscherer J, Beaulieu C, Stobbe R. Radiofrequency excitation-related ^{23}Na MRI signal loss in skeletal muscle, cartilage, and skin. *Magn Reson Med*. 2020;83(6):1992-2001. doi:10.1002/mrm.28054
18. Lommen J, Konstandin S, Kramer P, Schad LR. Enhancing the quantification of tissue sodium content by MRI: time-efficient sodium B_1 mapping at clinical field strengths. *NMR Biomed*. 2016;29(2):129-136. doi:10.1002/nbm.3292
19. Allen SP, Morrell GR, Peterson B, et al. Phase-sensitive sodium B_1 mapping. *Magn Reson Med*. 2011;65(4):1125-1130. doi:10.1002/mrm.22700
20. Gerhalter T, Gast LV, Marty B, Uder M, Carlier PG, Nagel AM. Assessing the variability of ^{23}Na MRI in skeletal muscle tissue: reproducibility and repeatability of tissue sodium concentration measurements in the lower leg at 3 T. *NMR Biomed*. 2020;33(5):e4279. doi:10.1002/nbm.4279
21. Noebauer-Huhmann IM, Juras V, Pfirrmann CW, et al. Sodium MR imaging of the lumbar intervertebral disk at 7 T: correlation with T2 mapping and modified Pfirrmann score at 3 T—preliminary results. *Radiology*. 2012;265(2):555-564. doi:10.1148/radiol.12111920
22. Wetterling F, Corteville DM, Kalayciyan R, et al. Whole body sodium MRI at 3T using an asymmetric birdcage resonator and short echo time sequence: first images of a male volunteer. *Phys Med Biol*. 2012;57(14):4555-4567. doi:10.1088/0031-9155/57/14/4555
23. Cunningham CH, Pauly JM, Nayak KS. Saturated double-angle method for rapid B_1+ mapping. *Magn Reson Med*. 2006;55(6):1326-1333. doi:10.1002/Mrm.20896
24. Harrington MG, Salomon RM, Pogoda JM, et al. Cerebrospinal fluid sodium rhythms. *Cerebrospinal Fluid Res*. 2010;7(3). doi:10.1186/1743-8454-7-3
25. Yarnykh VL. Actual flip-angle imaging in the pulsed steady state: a method for rapid three-dimensional mapping of the transmitted radiofrequency field. *Magn Reson Med*. 2007;57(1):192-200. doi:10.1002/Mrm.21120
26. Sacolick LI, Wiesinger F, Hancu I, Vogel MW. B_1 mapping by Bloch–Siegert shift. *Magn Reson Med*. 2010;63(5):1315-1322. doi:10.1002/mrm.22357
27. Morrell GR, Schabel MC. An analysis of the accuracy of magnetic resonance flip angle measurement methods. *Phys Med Biol*. 2010;55(20):6157-6174. doi:10.1088/0031-9155/55/20/008
28. Pohmann R, Budde J, Auerbach EJ, Adriany G, Ugurbil K. Theoretical and experimental evaluation of continuous arterial spin labeling techniques. *Magn Reson Med*. 2010;63(2):438-446. doi:10.1002/mrm.22243
29. Niesporek SC, Hoffmann SH, Berger MC, et al. Partial volume correction for in vivo ^{23}Na-MRI data of the human brain. *NeuroImage*. May 15 2015;112:353-363. doi:10.1016/j.neuroimage.2015.03.025
30. Solanky BS, Riemer F, Golay X, Wheeler-Kingshott CA. Sodium quantification in the spinal cord at 3T. *Magn Reson Med*. 2013;69(5):1201-1208. doi:10.1002/mrm.24696
31. Wang C, McArdle E, Fenty M, et al. Validation of sodium magnetic resonance imaging of intervertebral disc. *Spine*. 2010;35(5):505-510. doi:10.1097/BRS.0b013e3181b32d3b
32. Kraemer J, Kolditz D, Gowin R. Water and electrolyte content of human intervertebral discs under variable load. *Spine*. Jan-Feb 1985;10(1):69-71. doi:10.1097/00007632-198501000-00011
33. Trattnig S, Stelzeneder D, Goed S, et al. Lumbar intervertebral disc abnormalities: comparison of quantitative T2 mapping with conventional MR at 3.0 T. *Eur Radiol*. 2010;20(11):2715-2722. doi:10.1007/s00330-010-1843-2
34. Blumenkrantz G, Zuo J, Li X, Kornak J, Link TM, Majumdar S. In vivo 3.0-tesla magnetic resonance $T_{1\rho}$ and T_2 relaxation mapping in subjects with intervertebral disc degeneration and clinical symptoms. *Magn Reson Med*. 2010;63(5):1193-1200. doi:10.1002/mrm.22362
35. Barry RL, Vannesjo SJ, By S, Gore JC, Smith SA. Spinal cord MRI at 7T. *NeuroImage*. 2018;168:437-451. doi:10.1016/j.neuroimage.2017.07.003
36. Sengupta S, Welch EB, Zhao Y, et al. Dynamic B_0 shimming at 7 T. *Magn Reson Imaging*. 2011;29(4):483-496. doi:10.1016/j.mri.2011.01.002
37. Vannesjo SJ, Miller KL, Clare S, Tracey I. Spatiotemporal characterization of breathing-induced B0 field fluctuations in the cervical spinal cord at 7T. *NeuroImage*. 2018;167:191-202. doi:10.1016/j.neuroimage.2017.11.031
38. Bartha R, Menon RS. Long component time constant of ^{23}Na T_2^* relaxation in healthy human brain. *Magn Reson Med*. 2004;52(2):407-410. doi:10.1002/mrm.20144

How to cite this article: Çavuşoğlu M, Pazahr S, Ciritsis AP, Rossi C. Quantitative ^{23}Na-MRI of the intervertebral disk at 3 T. *NMR in Biomedicine*. 2022;35(8):e4733. doi:10.1002/nbm.4733